Paper

Experimental Evaluation of Switched Reluctance Motor Made by Blanking Amorphous Alloy Foil

Takahiro Kumagai*a) Student Member, Hirotaka Sakurai* Student Member,
Taisuke Shioi* Student Member, Hirotaka Kato* Student Member,
Jun-ichi Itoh* Senior Member, Keisuke Kusaka* Member,
Takashi Yamaguchi** Non-Member, Masayuki Nakagawa*** Non-Member,
Daisuke Sato**** Member

This study reveals the characteristics of switched reluctance motors (SRMs) made by blanking (a) 20HX1300 of high grade low-iron-loss silicon steel (0.20mm thickness) and (b) 2605SA1 of amorphous alloy (0.025mm thickness). The blanking of the amorphous alloy is an innovative technology for the mass production of the high efficiency amorphous-alloy-motor. The impact of the processing methods on the magnetic properties are evaluated using the ring cores processed by the following methods: the wire cutting and the blanking. On the other hand, the experiment with the SRMs processed by the blanking evaluates the characteristics depending on the material. As first prototype, 70W-SRM (40mm thickness) is manufactured by blanking 1600 sheets of the amorphous alloy and adhesively laminating them. In the experiment, the motor efficiency of the amorphous-alloy-SRM is improved by 6.9 p.t. compared with that of silicon-steel-SRM. In addition, the iron loss of amorphous-alloy-SRM is reduced by 78.7% compared with that of silicon-steel-SRM.

Keywords : Switched reluctance motor (SRM), ring core, finite element analysis (FEA), amorphous alloy foil, blanking, iron loss

1. Introduction

High-efficiency motor and high-power density motor for home appliances, industrial application, and electric vehicles have been actively studied and developed due to an increasing awareness of environmental issues [1-5]. The electric motor is operated at higher speed in order to achieve the higher power density. High speed operation has become easier with the practical use of wide bandgap semiconductors such as a silicon carbide (SiC) and a gallium nitride (GaN). However, high speed operation deteriorates the motor efficiency due to the iron loss which is increased depending on the electrical frequency.

Amorphous alloy has drawn much attentions thanks to its low iron loss properties. In the amorphous alloy, the eddy current loss is small because it is thin and high electrical resistivity. In addition, the hysteresis loss is also small because it has no crystal structure [6]. So far, there are many researches to apply the amorphous alloy into the core of classic motors such as a permanent magnetic

synchronous motor (PMSM) [7-11], an induction motor (IM) [12], and a switched reluctance motor (SRM) [13-15]. In particular, Ref.[15] has reported that the iron loss of motor core was reduced by about 80% compared with 35A300 of a general low-iron-loss silicon steel with the employment of amorphous alloy. In addition, the efficiency of this amorphous alloy motor achieved more than 95% at an output of about 2kW thanks to its low iron loss properties. However, wire electrical discharge machining (WEDM), laser cutting, or chemical etching is adopted as a cutting method of the amorphous alloy foil due to the difficulty in machining amorphous alloy. These cutting processes lead to increasing of manufacturing cost and become an obstacle of mass production of an amorphous alloy motor. As the researches for the mass production of the amorphous alloy motor, there are two different approaches; (i) improvement of motor structure in order to avoid the complicated cutting process or (ii) improvement of blanking technology.

In approach (i), the simplification of the motor structure has been studied for avoidance of complicated cutting process. Ref.[16-23] have focused on an axial-gap motor whose stator core is a cylinder with a uniform cross-section shape in the axial direction, where it is comparatively easy to manufacture with the amorphous alloy. In particular, Ref.[22] has already commercialized the amorphous alloy axial-gap motor which satisfies the IE4 efficiency class. In addition, IE5 efficiency class is achieved with the improved amorphous alloy axial-gap motor in Ref.[23]. However, these approaches still limit the applicability of the amorphous alloy.

In approach (ii), the cutting of the amorphous alloy foil has been attempted with the development of mold processing machines and technologies [24-30]. Ref.[28] has been reported that amorphous

---

a) Correspondence to: Takahiro Kumagai. E-mail: kumagai_t1125@stn.nagaokaut.ac.jp
* Nagaoka University of Technology,
   1603-1, Kamitomioka-machi, Nagaoka-shi, Niigata 940-2188, Japan
** Yamaguchi Manufacturing Co., Ltd.,
   10245-1, Katakai-machi, Ojiya-shi, Niigata 947-0101, Japan
*** Industrial Research Institute of Niigata Prefecture,
   1-11-1, Abuminishi, Niigata-shi Chuo-ku, Niigata 950-0915, Japan
**** Nagaoka Motor Development Co., Ltd.,
   16-2085, Nagaoka Business Incubation Center, Fukasawa-machi, Nagaoka-shi, Niigata, 940-2135, Japan

alloy foil was successfully blanked into a motor stator shape. In Ref.[29], the high-speed blanking of the amorphous alloy foil has been conducted and evaluated. Ref.[30] has presented the blanking results of the amorphous alloy stacks laminated by 20 layers. However, as far as the author knows, there is no instance to manufacture the entire motor by blanking amorphous alloy foil. In other words, the characteristics of the entire motor by blanking the amorphous alloy have not been revealed. The establishment of the blanking technologies of the amorphous alloy and the quantitative evaluation for the impact of the blanking process are expected in order to expand the application of the amorphous alloy more widely.

In this paper, an entire switched reluctance motor (SRM) is manufactured by blanking the amorphous alloy. The new contribution of this paper is experimental evaluation of the iron loss characteristic and motor efficiency characteristic of the manufactured SRM by blanking the amorphous alloy.

This paper is organized as follows; first, the impacts of the processing methods on the magnetic properties are evaluated with the ring cores processed by two methods: the wire cutting and the blanking; Next, the experiment with the SRMs processed by the blanking evaluates the characteristics depending on the material. As first prototype, 70WSRM (40mm thickness) is manufactured by blanking 1600 sheets of the amorphous alloy and adhesively laminating them. In addition, the same designed SRM is manufactured by blanking silicon steel for comparative verification. Note that this paper is the updated version of the conference paper [31]. The manuscript additionally evaluates the B-H characteristics and iron loss characteristics with ring cores, improves the accuracy of finite element analysis (FEA), and replaces all the old experimental results of 7200r/min with the new experimental results of 10000r/min.

2. Pre-experimental iron loss evaluation of ring cores

The B-H characteristics and the iron loss characteristics of the cores made by different material and different processing method are evaluated with ring cores as a preliminary step of the experimental evaluation with motor. Generally, the evaluation of the iron loss characteristic with ring core is more basic and more accurate.

2.1 Experimental preparation

Table.1 shows the specifications of the ring cores, whereas Fig.1 shows the photograph of the manufactured ring cores. Four ring cores are manufactured in order to evaluate the iron loss characteristics of the cores made by the different material and the different processing method. Two ring cores are made by the laser cutting after laminating (a) 20HX1300 of the high grade low-iron-loss silicon steel (0.20mm thickness) and (b) 2605SA1 of the amorphous alloy (0.025mm thickness), which are referred as "SS-C" and "AA-C" in this paper. The others are made by laminating after blanking (a) 20HX1300 and (b) 2605SA1, which are referred as "SS-B and "AA-B in this paper. The conductive elements of the laser cut surface of the manufactured SS-C and AA-C are removed with etching process in order to prevent the increase of the eddy current loss due to the short circuit between laminated steel sheets. Note that the lamination factor k_l is calculated from

$$k_l = \frac{m}{\rho_m V_{vol}} \text{.. (1)},$$

where m is the mass of the ring core, ρ_m is the density of the material,

Table 1. Specifications of ring-cores

Name of Ring core	SS-C	SS-B	AA-C	AA-B
Iron core	silicon steel (20HX1300)		amorphous alloy (2605SA1)	
Steel Thickness	0.20mm		0.025mm	
Processing Method	Wire cut* After Laminated	Laminated After Blanking	Wire cut* After Laminated	Laminated After Blanking
Lamination factor	95.9%	96.9%	93.1%	90.8%

* The conductive elements of wire cut surface are removed with etching process

Fig. 1. Photograph of ring-cores made with the processing methods as shown in Table 1.
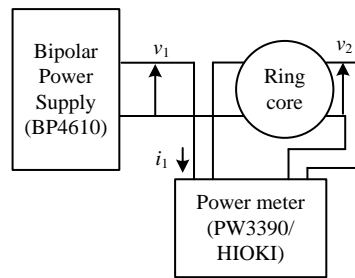
Fig. 2. Diagrams of measurement setup for ring-core

and V_{vol} is the volume of the ring core. As shown in Table 1, the lamination factors of AA-C and AA-B are a little worse than that of SS-C and SS-B. This deterioration of the lamination factor will be due to the thinner and the higher number of layers of the amorphous alloy than these of the silicon steel.

Fig.2 depicts the diagrams of the measurement setup for the ring core. The primary and secondary windings are wound around the manufactured ring core. The magnetic flux density $B(t)$ and the magnetizing force $H(t)$ are expressed as

$$B(t) = \frac{1}{N_2 S_c} \int_0^t v_2(t) dt \text{...(2)}$$

$$H(t) = \frac{N_1 i(t)}{l} \text{...(3)},$$

where $v_2(t)$ is the voltage of the secondary winding, N_2 is the number of turns in the secondary winding, S_c is the effective cross-sectional area of the ring core, $i_1(t)$ is the current in the primary winding, N_1 is the number of turns in the primary winding, and l is the effective magnetic path length of the ring core. On the other hand, the iron loss W_i and the amplitude of magnetic flux density B_m are expressed as
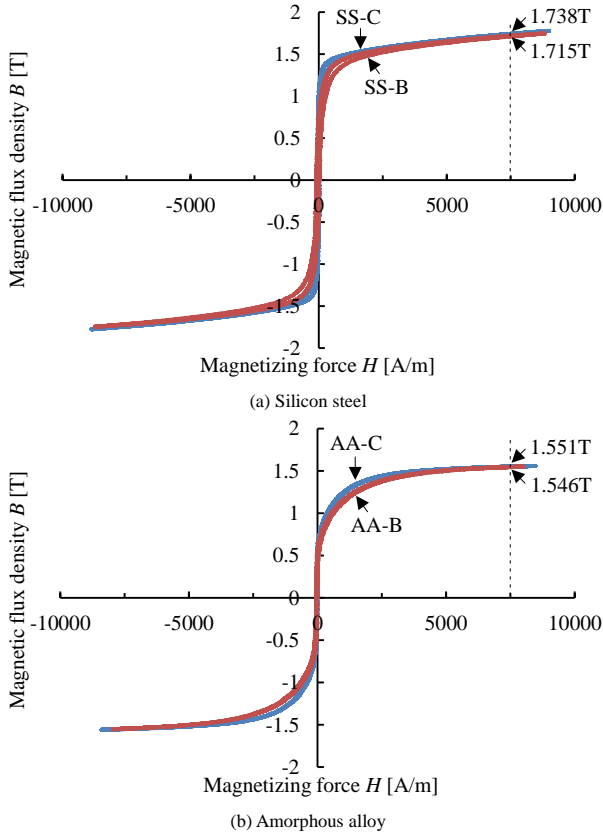
(a) Silicon steel

(b) Amorphous alloy

Fig. 3. Measured B-H characteristics at a frequency of 50Hz.

Table 2. Magnetic flux density at 7500A/m and permeability around 0A/m

	B_{75} (=B at 7500A/m)	μ_i (=dB/dH around 0A/m)
SS-C	1.738T	0.0195H/m
SS-B	1.715T	0.0117H/m
AA-C	1.551T	0.0241H/m
AA-B	1.546T	0.0195H/m

$$W_i = \frac{1}{T}\int_0^T i_1(t)v_2(t)dt \quad\text{..(4)}$$

$$B_m = \frac{\sqrt{2}V_{2\_rms}}{2\pi f N_2 S_c} \quad\text{.. (5),}$$

where f is the frequency of the applied sinusoidal voltage, V_{2_rms} is the root mean square value of $v_2(t)$ at no-load test. Note that $v_2(t)$ is not the value converted to the voltage of the primary winding, but the measured value of the voltage of the secondary winding. The active power measured by the power meter in Fig.2, i.e. the time average value of instantaneous power expressed by (4), is equal to the magnetic energy consumed by the iron core.

2.2 Measurement results of B-H characteristic

Fig.3 shows the measured B-H characteristics, whereas Table 2 shows the magnetic flux density at 7500A/m (which is defined as B_{75}) and the permeability around 0A/m (which is defined as μ_i). The frequency of the applied sinusoidal voltage is low frequency of 50Hz in order to avoid the effects of the eddy current loss. B_{75} of AA-C and AA-B are 10.8% and 9.9% lower than that of SS-C and SS-B respectively in regard to the difference in the characteristics depending on the material. In addition, μ_i of AA-C and AA-B are 23.6% and 66.7% higher than that of SS-C and SS-B respectively.

(a) Silicon steel
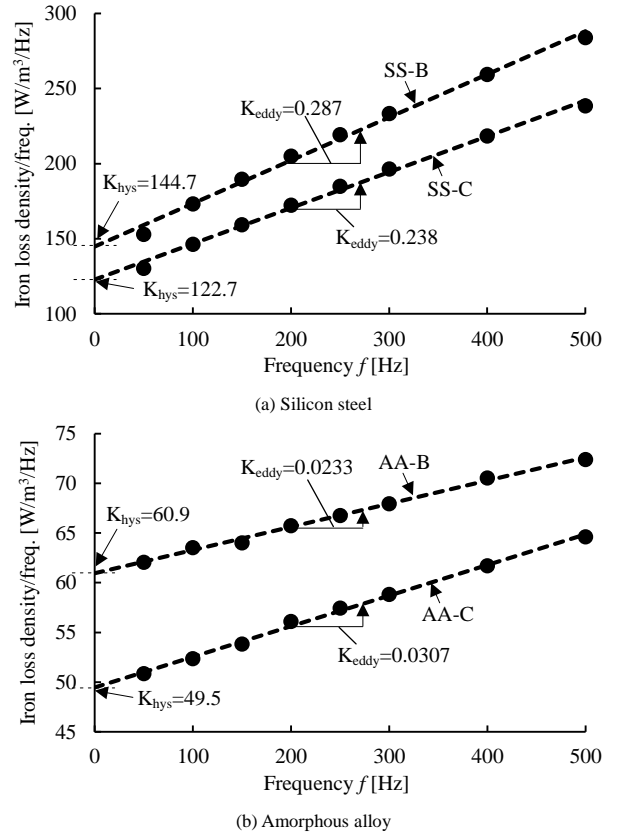
(b) Amorphous alloy

Fig. 4. Measured iron loss characteristics at 1.0T.

Table 3. Coefficients of the Steinmetz equation

	$K_{hys.}$	$K_{eddy.}$
SS-C	122.7	0.238
SS-B	144.7	0.287
AA-C	49.5	0.0307
AA-B	60.9	0.0233

Therefore, the amorphous alloy has slightly lower magnetic flux density and higher permeability compared with the silicon steel. B_{75} of SS-B and AA-B are decreased by only 1.3% and 0.3% respectively compared with that of SS-C and AA-C in regard to the difference in the characteristics depending on the processing process. In addition, μ_i of SS-B and AA-B are decreased by 40.0% and 19.1% respectively compared with that of SS-C and AA-C. Therefore, the blanking process has little effect on the magnetic flux density, but it decreases the permeability. This decrease of the permeability will be due to the properties degradation with plastic strain and elastic strain generated at the end of the steel sheet during the blanking processes. However, μ_i of AA-B is still same level as that of SS-C in spite of the properties degradation.

2.3 Experimental results of iron loss characteristic

Fig.4 shows the measured iron loss characteristic at 1.0T, whereas Table 3 shows the coefficients of the Steinmetz equation. The frequency of the applied sinusoidal voltage is low frequency of from 50Hz to 500Hz in order to evaluate the eddy current loss not including the skin effect which occurs in the high frequency region. The Steinmetz equation is expressed as

$$W_i = K_{hys} f B_m^{\alpha_{hys}} + K_{eddy} f^2 B_m^2 \quad\text{.....................................(6),}$$

where α_{hys}, K_{hys} and K_{eddy} represents the coefficients of the hysteresis loss and the eddy current loss. K_{hys} and K_{eddy} are

calculated as the intercept and slope of W_i / f at $B_m = 1$T as shown in Fig.4. K_{eddy} of AA-C and AA-B are 87.1% and 91.9% lower than that of SS-C and SS-B respectively in regard to the difference in the characteristics depending on the material. Therefore, the eddy current loss of the amorphous alloy is expected to be 1/10 of the silicon steel at the same f and the same B_m. In addition, K_{hys} of AA-C and AA-B are 59.7% and 57.9% lower than that of SS-C and SS-B respectively. Therefore, the hysteresis loss of the amorphous alloy is expected to be less than 1/2 of the silicon steel at the same f and the same $B_m = 1$[T] (because of $B_m^{dhys}=1$). K_{eddy} of SS-B is increased by 20.6% compared with that of SS-C, whereas K_{eddy} of AA-B is decreased by 24.1% compared with that of AA-C in regard to the difference in the characteristics depending on the processing process. This will be due to the following two factor; (i) the increase of the eddy current loss due to the remaining conductive elements of the wire cut surface which could not be removed even by etching process in SS-C and AA-C and (ii) the properties degradation with the plastic strain and elastic strain generated at the end of the steel sheet during the blanking processes in SS-B and AA-B. In the silicon steel, the impact of (i) is greater than that of (ii). On the other hand the amorphous alloy, the impact of (i) is smaller than that of (ii). On the other hand, K_{hys} of SS-B and AA-B are increased by 17.9% and 23.0% compared with that of SS-C and AA-C. This will be due to the factor (ii). Therefore, the blanking process has little effect on the eddy current loss, but it increases the hysteresis loss. This increase of the hysteresis loss is a problem in the electrical properties of the blanked material. Note that the eddy current loss dominates the iron loss of the high-speed motor. Therefore, the properties degradation due to blanking the amorphous alloy is not a serious problem in practical use.

3. Improvement of accuracy of iron loss analysis in FEA

It was confirmed that the accuracy of FEA is low in the simple iron loss calculation algorithm based on the iron loss curve [31]. This is because the analysis based on the iron loss curve is not applicable into the complicated magnetic flux waveforms of the SRM. In this paper, the hysteresis loss is analyzed based on Play Model [32-33], whereas the eddy current loss is analyzed by Homogenization method [34-35]. These methods are higher accuracy than that based on the iron loss curve thanks to the consideration of the DC bias characteristics of the hysteresis loss and the skin effect of the eddy current loss [36-37].

3.1 Preparation of Play model based method

Fig.5 shows the measured hysteresis curves of AA-B. The play model is the magnetization model which reproduces any minor loop. The hysteresis loss is calculated from the history of magnetization, i.e. the area of the B-H loop. This method is performed considering the DC bias characteristics of hysteresis loop. It is necessary for Play model to prepare a group of major B-H loops with different amplitude as shown in Fig.5. These B-H loops are measured by the method as explained in Subsection 2.2. The measurement range is from 0.05T to 1.90T for 20HX1300, and from 0.05T to 1.55T for 2605SA1. These measured data were implemented in JMAG Designer.

3.2 Preparation of Homogenization method

Table 4 shows the characteristic of 20HX1300 and 2605SA1. The classical eddy current loss W_{eddy_cla} is calculated from the thickness d and electrical resistivity ρ of the electrical sheet in the homogenization method. The values of d and ρ are the catalog value

(a) Entire (±15000A/m, ±2T)
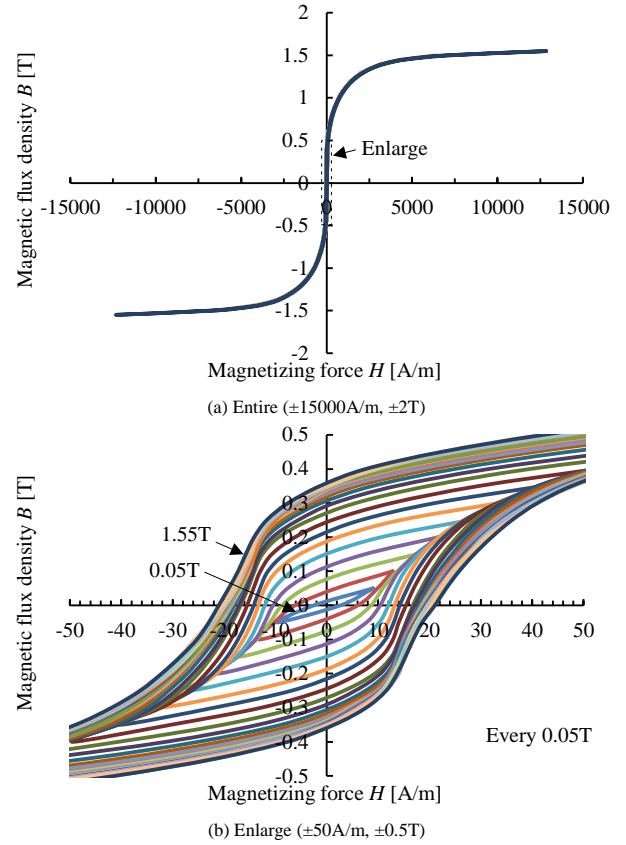
(b) Enlarge (±50A/m, ±0.5T)
Fig. 5. Measured hysteresis loops of AA-B

Table 4. Characteristic of 20HX1300 and 2605SA1

	d [mm]	p [$10^{-6}\Omega$m]	K_{eddy}	κ
20HX1300(SS-B)	0.2	0.55	0.287	2.40
2605SA1(AA-B)	0.025	1.3	0.0233	29.5

[38-39] in this paper. This method is performed considering the skin effect of the eddy current loss. Note that the classical eddy current loss calculated by the homogenization method does not include the excess loss such as anomalous eddy current loss. Therefore, the modified coefficient κ of the classical eddy current loss is defined as

$$\kappa = \frac{K_{eddy} f^2 B_m^2}{\frac{(\pi f d B_m)^2}{6p}} = \frac{K_{eddy}}{\frac{(\pi d)^2}{6p}} \quad \text{...(7),}$$

where K_{eddy} represents the coefficients of the eddy current loss which does not include the skin effect as explained in Subsection 2.3. The eddy current loss W_{eddy} including the excess loss W_{eddy_ex} is expressed as

$$W_{eddy} = W_{eddy\_cla} + W_{eddy\_ex} = \kappa W_{eddy\_cla} \quad \text{............................(8).}$$

Therefore, the eddy current loss is calculated by multiplying the analysis value of the classical eddy current loss by the modified coefficient κ. As shown in Table.4, the κ of the blanked silicon steel is 2.40, whereas the κ of the blanked amorphous alloy is 29.5. There is a pretty difference between the actual eddy current loss and the eddy current loss calculated by the physical property such as the thickness and electrical resistivity in the blanked amorphous alloy.

4. Design and Manufacture of SRMs

Table.5 shows the specifications of the designed SRMs, whereas Fig.6 shows the photograph of the manufactured amorphous-allow-

Table 5. Specifications of test SRMs

Name of motor	SS-SRM	AA-SRM
Iron core	20HX1300 (high grade silicon steel)	2605SA1 (amorphous alloy)
Number of layers	200 (cal.)	1600 (cal.)
Processing method	Laminated after Blanking	
Output power	70W	
Maximum speed	10000r/min	
Number of phases	3	
Number of poles	6 (stator) / 4 (rotor)	
Motor size	40mm × 40mm	
Airgap	0.1mm	
Pole arc	21deg. (stator) / 31deg. (rotor)	
Number of turns	73turns	
Space factor of coil	34%	

Fig. 6. Photograph of 70W-SRM made of blanked amorphous alloy foil.

SRM. 70W SRMs (40mm thickness) are designed as first prototype. Two motor cores are made by blanking (a) 20HX1300 and (b) 2605SA1, which are referred as "SS-SRM" and "AA-SRM" in this paper. The detail of the employed innovative technology in blanking of the amorphous alloys is found in Ref.[40]. The comparative evaluation of the electrical characteristics of the different blanking technologies will be discussed in a future work. Note that the stator outer diameters of the blanked motor core are 40mm. There are problems of the material availability and the mold precision in order to blank larger motor core. The number of layers of SS-SRM is 200, whereas that of AA-SRM is 1600. These motors are manufactured by adhesively laminating the blanked steel sheets. Since it is difficult to laminate very thin steel sheets of the amorphous alloy with a caulking or a welding, an impregnation lamination is employed. There is a problem of the lower productivity due to the requirement of the manufacturing time for the adhesion process. In order to increase the effect of the iron loss reduction, a relatively high-speed motor is designed. In addition, the coil space is bigger than that of a general design [41] in order to increase the winding diameter. This results in low winding resistance and copper loss reduction. Furthermore, the airgap length is selected in order to achieve the highest efficiency within the mechanical constraint of 0.1 mm.

Fig.7(a) depicts the relationship between the airgap length and the motor loss, whereas Fig.7(b) shows the relationship between the airgap length and the motor efficiency. As shown in Fig.7(a), the large airgap extremely increases the copper loss. This is because the reluctance torque becomes small due to small change of the magnetic resistance with the change of the airgap length. The

(a) Motor loss
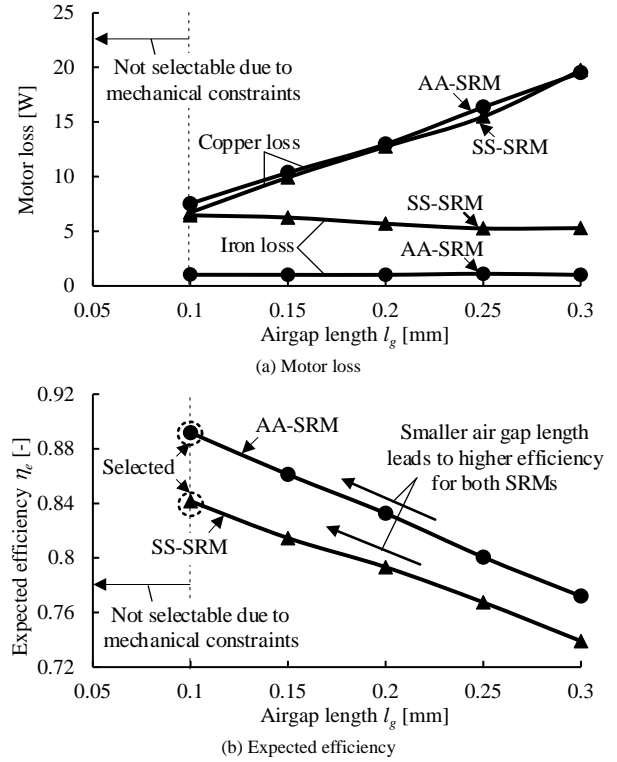
(b) Expected efficiency
Fig. 7. Effect of airgap length

Table 6. Cost comparison in different processing methods excluding the cost of molds and equipment

	Wire cure After Laminated	Laminated After Blanking
Silicon steel	K_{SS-B}	$K_{SS-B} \times 1/30 \sim 1/50$
Amorphous alloy	K_{AA-B}	$K_{AA-B} \times 1/10$

Table 7. Cost comparison of blanking processing in different materials

	Silicon steel	Amorphous alloy
	Laminated After Blanking	
Material price	K_{SS-M}	$K_{SS-M} \times 2$
Jig tool costs	K_{SS-J}	$K_{SS-J} \times 3 \sim 5$
Re-polishing cost	K_{SS-R}	$K_{SS-R} \times 30 \sim 50$
Assembly cost	K_{SS-A}	$K_{SS-A} \times 30 \sim 50$

copper loss of AA-SRM remains almost the same to that of SS-SRM. Therefore, the high efficiency is not expected due to small effect of reducing the motor loss with the low iron loss characteristics of the amorphous alloy. In this paper, the airgap length in both SS-SRM and AA-SRM are selected to be 0.1mm in order to achieve the highest efficiency within the mechanical constraint.

The information about the cost, structural strength, and heat-resistant are described. Note that the main subject of this paper is the evaluation of the electrical characteristics of the motors made by blanking the amorphous alloy. Therefore, the information about the cost and other are described as reference values.

Table.6 shows the cost comparison in the different processing methods excluding the cost of the molds and the manufacturing equipment. The cost reduction by the blanking of the silicon steel in the mass production is expected to be 1/30~1/50 compared with that of the wire cutting. On the other hand, that of the amorphous alloy is expected to be 1/10 due to the larger number of required

sheets and the difficulty of processing of amorphous alloy.

Table.7 shows the cost comparison of blanking processing in the different materials. The material cost of the amorphous alloy is expected to be increased by 2 times compared with that of the silicon steel [42]. In addition, the jig tool cost is expected to be increased by from 3 times to 5 times. This is because the clearance of the jig tool is very small, and the required accuracy of the jig tools is very high. In addition, the re-polishing cost is expected to be increased by from 30 times to 50 times. This is because not only the number of required sheets is larger but also the tensile strength is high in the amorphous alloy. In addition, the assembly cost is expected to be increased by from 30 times to 50 times because of the large number of required sheets, more frequently re-polishing, and the manufacturing time for the adhesion process in the impregnation lamination.

The structural strength of the motor made by blanking the amorphous alloy is higher than that of the silicon steel. This is because the structural strength depends on the hardness of the core. The hardness of the amorphous is approximately 5 times higher than that of the silicon steel. On the other hand, the heat-resistant is expected to be same.

5. Experimental evaluation of SRMs

5.1 Test system configuration

Fig.8 (a) depicts the diagrams of the measurement setup for test motor, whereas Fig.8 (b) shows the photograph of the measurement bench. In particular, the motor efficiency characteristics and the iron loss characteristics of SS-SRM and AA-SRM are experimentally evaluated with the measurement bench. The input electric power and the root-mean-square (RMS) value of the winding current are measured with the power meter (PW3390, accuracy ±0.04%, bandwidth 200kHz, HIOKI), whereas the torque is measured with the torque meter (UTMII-1Nm, accuracy±0.01%, bandwidth1kHz, UNIPULSE). The winding temperature is measured by thermocouple built into the winding.

The motor efficiency η_m is expressed as

$$\eta_m = \frac{P_{out}}{P_{in}} = \frac{T_{out}\omega_m}{P_{in}} \quad\cdots\cdots\cdots\cdots\cdots (9),$$

where P_{out} is the shaft output which is calculated as product of the measured torque T_{out} and the shaft angular velocity ω_m, whereas P_{in} is the input electric power which is measured by the power meter. According to the preliminary verification in Ref.[31], the mechanical loss has large dispersion. In addition, there are individual differences of mechanical loss in SS-SRM and AA-SRM. Therefore, it is impossible for the evaluation with Eq.(9) to make a fair comparison. In order to resolve the above problems, the efficiency η_e regarding the mechanical loss as a part of the shaft output is defined as

$$\eta_e = \frac{P_{out\_m}}{P_{in}} = \frac{P_{out} + W_m}{P_{in}} = \frac{T_{out}\omega_m + T_{mech}\omega_m}{P_{in}} \quad\cdots\cdots\cdots (10),$$

where P_{out_m} is the shaft output when the mechanical loss W_m is regarded as shaft output. Note that W_m is the product of the measured torque T_{mech} and the rotational angular velocity ω_m when the DC motor drives the system with no SRM excitation. On the other hand, the iron loss W_i is calculated by subtracting P_{out}, W_m, and the copper loss W_c from P_{in}. Therefore, W_i is expressed as
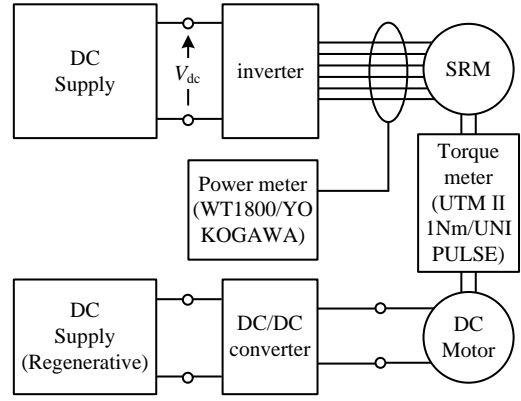
(a) Diagrams of measurement setup for test SRM
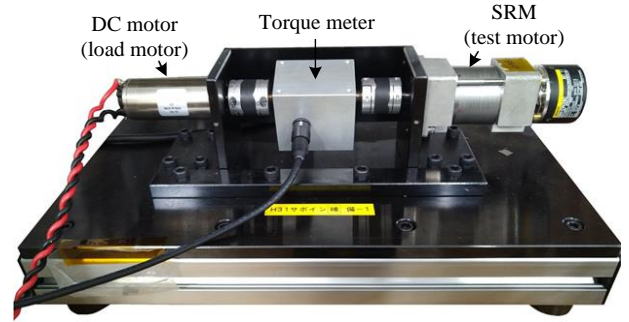
(b) Photograph of measurement bench

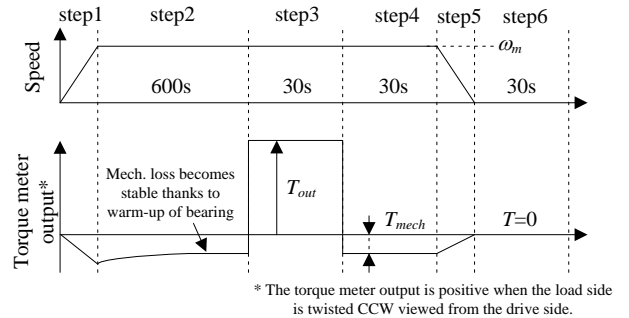Fig. 8. Measurement system for test SRM

* The torque meter output is positive when the load side is twisted CCW viewed from the drive side.

Fig. 9. The speed and the torque meter output during the experiment (Step1~Step6)

Table 8. The operation of load motor and test motor at each step

	Load motor	Test motor	Purpose
Step1	Acceleration	No excitation	-
Step2	ASR	No excitation	Warm-up of bearing
Step3	ASR	ACR	Output measurement
Step4	ASR	No excitation	Mech. loss measurement
Step5	Deceleration	No excitation	-
Step6	No excitation	No excitation	Zero point confirmation

$$W_i = P_{in} - P_{out} - W_c - W_m$$
$$= P_{in} - T_{out}\omega_m - \sum_{x=u}^{w} R_x(t_{temp})I_{RMS\_x}^{2} - T_{mech}\omega_m \quad\cdots\cdots\cdots\cdots(11),$$

where $R_x(t_{temp})$ is the winding resistance of x-phase respectively at winding temperature t_{temp}, whereas I_{RMS_x} is the root-mean-square (RMS) value of the winding current of x-phase respectively.

5.2 Test procedure

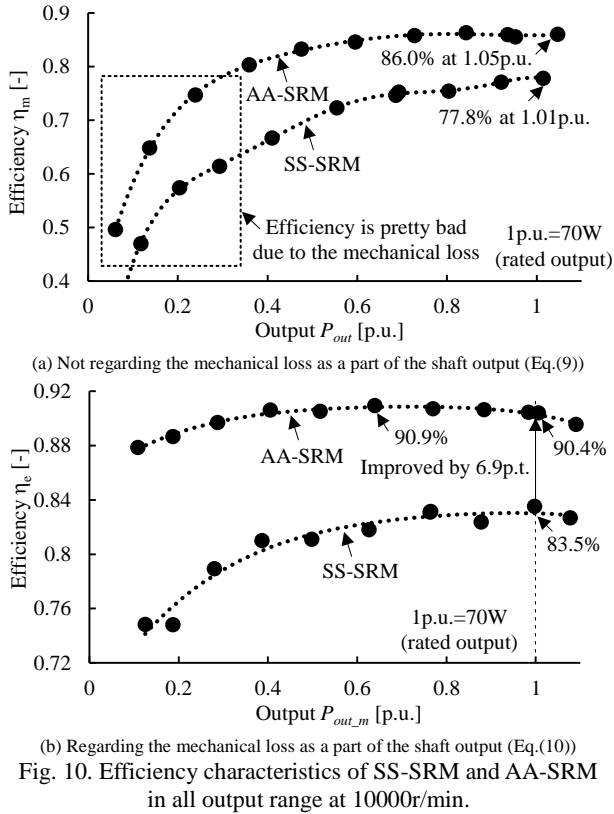The copper loss (winding resistance) depends on the winding

(a) Not regarding the mechanical loss as a part of the shaft output (Eq.(9))

(b) Regarding the mechanical loss as a part of the shaft output (Eq.(10))

Fig. 10. Efficiency characteristics of SS-SRM and AA-SRM in all output range at 10000r/min.

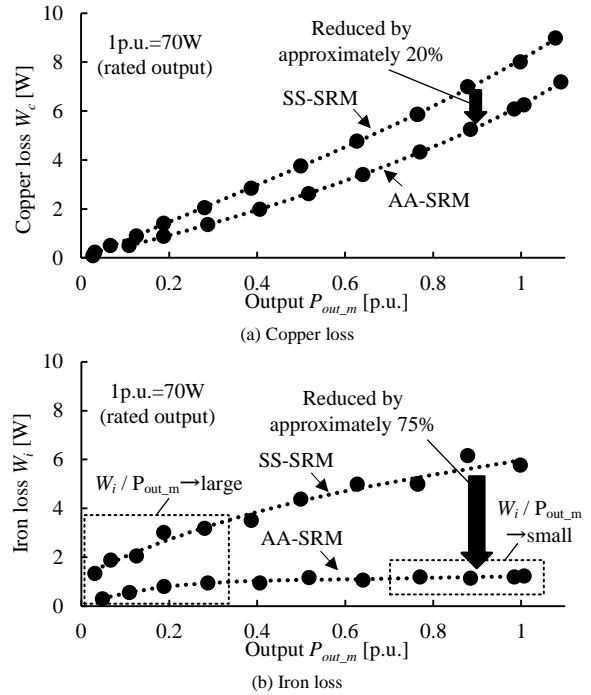(a) Copper loss

(b) Iron loss

Fig. 11. Motor loss comparison between SS-SRM and AA-SRM in all output range at 10000r/min.

Fig. 12. Motor loss comparison between SS-SRM and AA-SRM of rated power (70W) at 10000r/min.

temperature, whereas the mechanical loss depends on the bearing temperature. In particular, the bearing temperature cannot be measured in this system. Therefore, a warm-up operation is required in order to sufficiently warm the bearing.

Fig.9 shows the speed and the torque during the experiment (Step1~Step6), whereas Table8 shows the operation of load motor and test motor at each step. At first, the motor is accelerated by load motor (Step1). Next, the load motor drives the system with no SRM excitation for a long time (Step2). In Step2, the mechanical loss becomes stable thanks to warm-up of bearing. Next, the test motor output the torque by controlling the current to the pulse current with the command amplitude (Step3). In Step3, the efficiency and iron loss are calculated from the average value of the measured value in this section. Next, the load motor drives the system with no SRM excitation again (Step4). In Step4, the mechanical loss is calculated from the average value of the measured value in this section. Finally, the motor is decelerated (Step5) and stop (Step6). The zero point of the torque meter is confirmed in the stopped state (Step6).

5.3 Measured characteristics of SS-SRM and AA-SRM

Fig.10 shows the motor efficiency characteristics of SS-SRM and AA-SRM at 10000r/min. The mechanical loss is not regarded as a apart of the shaft output (i.e. use of Eq.(9)) in Fig.10(a), whereas the mechanical loss is regarded as a apart of the shaft output (i.e. use of Eq.(10)) in Fig.10(b). As shown in Fig.10(a), the motor efficiency of AA-SRM is higher than that of SS-SRM in all output range. In addition, AA-SRM achieved the maximum motor efficiency of 86.0% at 1.05p.u. of rated power (70W). In the low torque region, the efficiency is pretty bad due to the mechanical loss. As shown in Fig.10(b), the motor efficiency of AA-SRM is approximately 90% in all output range. In addition, AA-SRM achieved the motor efficiency of 90.4% at rated power (70W). At this operating point, the motor efficiency of AA-SRM is improved by 6.9 p.t. compared with that of SS-SRM.
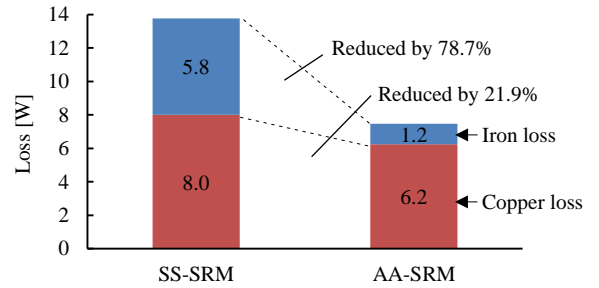
Fig.11 shows the comparison results of (a) the copper loss and (b) the iron loss of SS-SRM and AA-SRM. As shown in Fig.11(a), the copper loss of AA-SRM is reduced by approximately 20% compared with that of SS-SRM. In addition, as shown in Fig.11(b), the iron loss of AA-SRM is reduced by approximately 75% compared with that of SS-SRM. Note that the increase in the iron loss of AA-SRM decreases at high output, i.e. W_i / P_{out_m} becomes low. This is because the increase of the magnetic density decreases at high output due to the magnetic saturation of the amorphous alloy. In addition, the increase in the iron loss increases at low output, i.e. W_i / P_{out_m} becomes high. In the current hysteresis control with a constant hysteresis width, the iron loss due to the switching of the inverter is almost same, i.e. the influence becomes relatively large in the low output.

Fig.12 shows the comparison result of motor loss at rated power (70W). As shown in Fig.12, the copper loss of AA-SRM is reduced by 21.9% compared with that of SS-SRM. On the other hand, the iron loss of AA-SRM is reduced by 78.7% compared with that of SS-SRM. Therefore, it is confirmed that the iron loss reduction effect of the motor core with the amorphous alloy is high even in the blanked amorphous alloy.
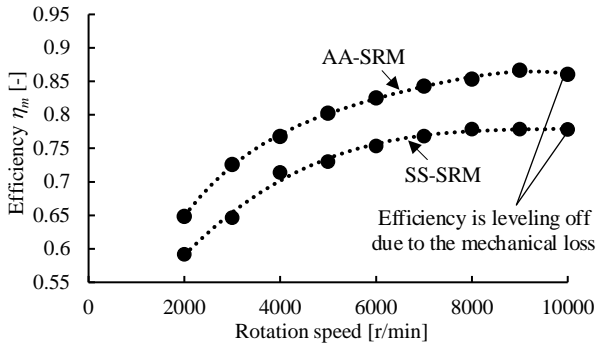
(a) Not regarding the mechanical loss as a part of the shaft output (Eq.(9))
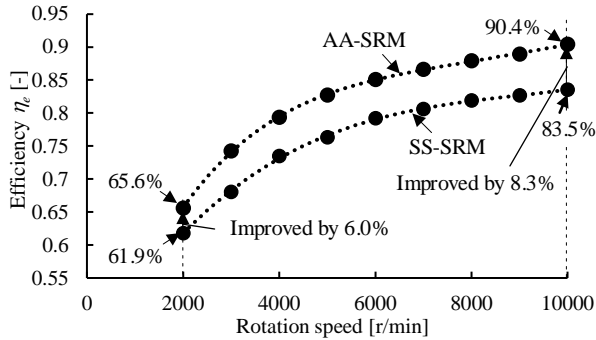
(b) Regarding the mechanical loss as a part of the shaft output (Eq.(10))

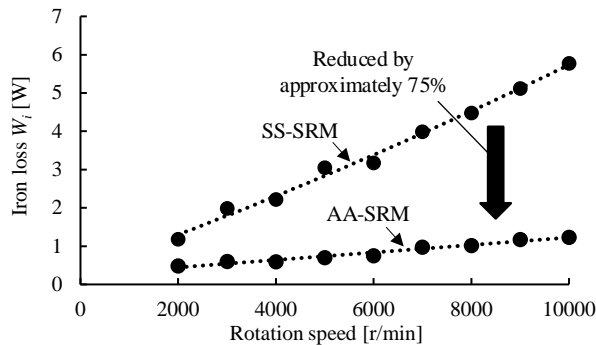Fig. 13. Efficiency characteristics of SS-SRM and AA-SRM in all speed range at 1p.u. torque.

Fig. 14. Iron loss characteristics of SS-SRM and AA-SRM in all speed range at 1p.u. torque.

Fig.13 shows the motor efficiency characteristics of SS-SRM and AA-SRM in all speed range at 1p.u. torque. The mechanical loss is not regarded as a part of the shaft output (i.e. use of Eq.(9)) in Fig.13(a), whereas the mechanical loss is regarded as a part of the shaft output (i.e. use of Eq.(10)) in Fig.13(b). As shown in Fig.13(a)(b), the motor efficiency of AA-SRM is higher than that of SS-SRM in all speed range. In addition, as shown in Fig.13(a), the motor efficiency is leveling off at approximately 10000 r/min due to the mechanical loss. As shown in Fig.9(b), the motor efficiency of AA-SRM is improved by 8.3% compared with that of SS-SRM at 10000r/min, while the motor efficiency of AA-SRM is improved by 6.0% compared with that of SS-SRM at 2000r/min. Therefore, the efficiency improvement thanks to the low iron loss characteristic of the amorphous alloy becomes greater at higher speeds.

Fig.14 shows the iron loss characteristics of SS-SRM and AA-SRM in all speed range at 1p.u. torque. The iron loss of AA-SRM is reduced by approximately 75% compared with that of SS-SRM in all speed range.
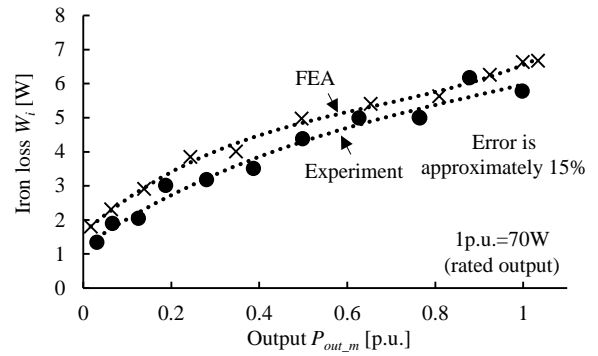
(a) SS-SRM
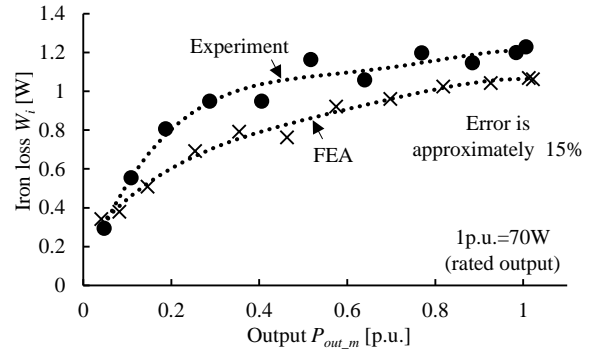
(b) AA-SRM

Fig. 15. Comparison results of measurement and FEA in all output range at 10000r/min.

5.4   Comparison results between measurement and FEA
Fig.15 shows the comparison between the measurement results and the FEA results of the iron losses of (a) SS-SRM and (b) AA-SRM. As shown in Fig.15, there is an error of approximately 15% between the measurement results and the FEA results in both SS-SRM and AA-SRM. These errors will be due to the accuracy of FEA analysis and the accuracy of measurement results. The characteristics of the blanked SRM is analyzed from the data of the characteristics of the blanked ring cores. However, the impact of the blanking process will be not always the same as that of the ring core, especially in complicated parts such as motor teeth. In addition, the iron loss in measurement results is the value calculated indirectly from other measured values by Eq.(11). However, there are errors in the value calculated iron loss due to the unconsidered loss such as the stray load loss and the AC copper loss.

Fig.16 shows the separation results of the iron loss of (a) SS-SRM and (b) AA-SRM at rated power (70W). The errors between the measurement results and the FEA results are 15% or less in both SS-SRM and AA-SRM. In SS-SRM, the eddy current loss is 59.9%, whereas the hysteresis loss is 40.1% of 5.77W of the total iron loss. On the other hand, in AA-SRM, the eddy current loss is 25.5%, whereas the hysteresis loss is 74.5% of 1.23W of the total iron loss. Therefore, the eddy current loss dominates the iron loss in SS-SRM, whereas the hysteresis loss dominates the iron loss in AA-SRM. In general, the eddy current loss dominates the iron loss of the general high-speed motor as shown in Fig.16(a) since the eddy current loss is proportional to the square of the electrical frequency. In the amorphous alloy, the eddy current loss is 1/10 and the hysteresis loss is 1/2 compared with the silicon steel. Therefore, the dominant eddy current loss at high-speed motor is dramatically reduced.

6. Conclusion

This paper provided the characteristics of the ring cores and the switched reluctance motors (SRMs) made by blanking (a) 20HX1300 of the high grade low-iron-loss silicon steel (0.20mm thickness) and (b) 2605SA1 of the amorphous alloy (0.025mm thickness). The blanking of the amorphous alloy is an innovative technology for the mass production of the high efficiency amorphous-alloy-motor. The impacts of the processing methods on the magnetic properties were evaluated with the ring cores processed by two methods: the wire cutting and the blanking. On the other hand, the experiment with the SRMs processed by the blanking evaluated the characteristics depending on the material. As first prototype, 70W-SRM (40mm thickness) was manufactured by blanking 1600 sheets of the amorphous alloy and adhesively laminating them. These experiments reveal the following characteristics of the entire motor by blanking the amorphous alloy:

(i) the amorphous alloy is expected to be 1/10 of the eddy current loss and 1/2 of hysteresis loss compared with the silicon steel according to the measured parameters of Steinmetz equation.

(ii) the hysteresis loss is expected to dominate of the iron loss in the amorphous ally motor even with the high speed operation.

(iii) the blanking of the amorphous alloy impacts the hysteresis loss rather than the eddy current loss, which is the important factor for the high efficiency with the high speed operation.

(iv) the blanking of the amorphous alloy is expected to increase the hysteresis loss by 23.0% according to the measured parameters of Steinmetz equation, which is not a serious problem in practical use.

(v) the iron loss of the amorphous-alloy-SRM was greatly reduced by compared with that of the silicon-steel-SRM. In addition, the motor efficiency of the amorphous-alloy-SRM is improved compared with that of the silicon-steel-SRM.

References

(1) Y. Enomoto, K. Deguchi, T. Imagawa, "Development of an Ultimate-high-efficiency Motor by utilizing High-Bs Nanocrystalline Alloy," IEEJ Journal of Industry Applications, vol. 9, no .1, pp. 102-108 (2020)

(2) T. Ogawa, T. Takahashi, M. Takemoto, S. Ogasawara, H. Arita, and A. Daikoku, "Increasing the Operating Speed of a Consequent Pole Axial Gap Motor for Higher Output Power Density," IEEJ Journal of Industry Applications, vol. 8, no. 3, pp. 497-504 (2019)

(3) U. U. Ekong, M. Inamori, and M. Morimoto, "Field-Weakening Control for Torque and Efficiency Optimization of a Four-Switch Three-Phase Inverter-Fed Induction Motor Drive," IEEJ Journal of Industry Applications, vol. 8, no. 3, pp. 548-555 (2019)

(4) K. Abe, H. Haga, K. Ohishi, Y. Yokokura, and H. Kada, "Source Current Harmonics and Motor Copper Loss Reduction Control of Electrolytic Capacitor-less Inverter for IPMSM Drive," IEEJ Journal of Industry Applications, vol. 8, no. 3, pp. 404-412 (2019)

(5) N. Miyauchi, "Reduction of the Power Consumption of a Stepping Motor for Driving the Hands of Wristwatches," IEEJ Journal of Industry Applications, vol. 8, no. 1, pp. 140-141 (2019)

(6) R. Tang, W. Tong, and X. Han, "Overview on amorphous alloy electrical machines and their key technologies," Chinese Journal of Electrical Engineering, vol. 2, no. 1, pp. 1–12 (2016)

(7) R. Kolano, A. Kolano-Burian, K. Krykowski, J. Hetmańczyk, M. Hreczka, M. Polak, and Jan Szynowski "Amorphous soft magnetic core for the stator of the high-speed PMBLDC motor with half-open slots," IEEE Transactions on Magnetics, vol. 52, no. 6, no. 2003005 (2016)

(8) S. Okamoto, N. Denis, Y. Kato, M. Ieki, and K. Fujisaki, "Core loss reduction of an interior permanent-magnet synchronous motor using amorphous stator core," IEEE Transactions on Industry Applications, vol. 52, no. 3, pp. 2261–2268 (2016)

(9) D.-K. Hong, D. Joo, B.-C. Woo, Y.-H. Jeong, and D.-H. Koo, "Investigations on a super high speed motor-generator for microturbine applications using
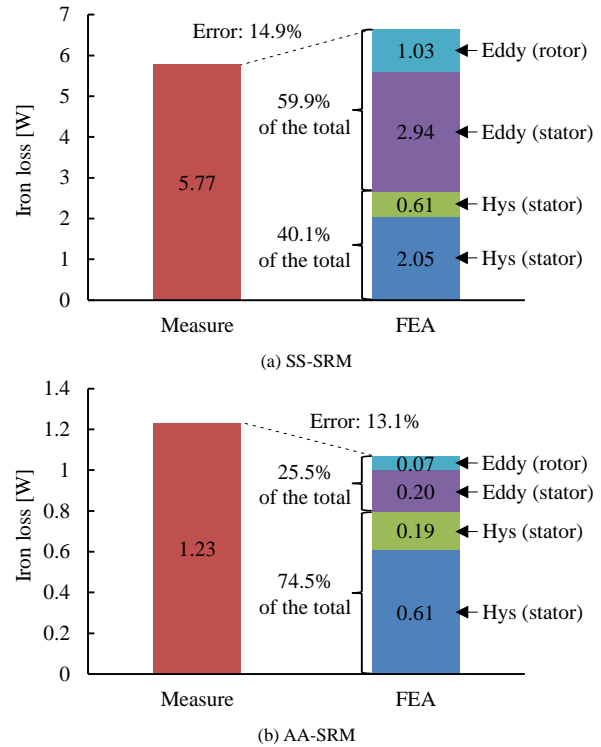
(a) SS-SRM

(b) AA-SRM

Fig. 16. Iron loss separation results of rated power (70W) at 10000r/min.

amorphous core," IEEE Transactions on Magnetics, vol. 49, no. 7, pp. 4072–4075 (2013)

(10) T. Fan, Q. Li, and X. Wen, "Development of a high power density motor made of amorphous alloy cores," IEEE Transactions on Industrial Electronics, vol. 61, no. 9, pp. 4510–4518 (2014)

(11) W. Tong, S. Dai, S. Wu, and R. Tang, "Performance Comparison Between an Amorphous Metal PMSM and a Silicon Steel PMSM," IEEE Transactions on Magnetics, vol. 55, no. 6, no. 8102705 (2014)

(12) M. Dems and K. Komeza, "Performance characteristics of a high-speed energy-saving induction motor with an amorphous stator core," IEEE Transactions on Industrial Electronics, vol. 61, no. 6, pp. 3046–3055 (2014)

(13) F. Chai, Z. Li, L. Chen, and Yulong Pei, "Effect of cutting and slot opening on amorphous alloy core for high-speed switched reluctance motor," IEEE Transactions on Magnetics, pp. 1–5 (2020)

(14) H. Hayashi, K. Nakamura, A. Chiba, T. Fukao, K. Tungpimolrut, and D. G. Dorrell, "Efficiency improvements of switched reluctance motors with high-quality iron steel and enhanced conductor slot fill," IEEE Transactions on Energy Conversion, vol. 24, no. 4, pp. 819–825 (2009)

(15) A. Chiba, H. Hayashi, K. Nakamura, S. Ito, K. Tungpimolrut, T. Fukao, M. A. Rahman, and M. Yoshida "Test results of an SRM made from a layered block of heat-treated amorphous alloys," IEEE Transactions on Industry Applications, vol. 44, no. 3, pp. 699–706 (2008)

(16) Z. Wang, Y. Enomoto, M. Ito, R. Masaki, S. Morinaga, H. Itabashi, S. Tanigawa, "Development of a permanent magnet motor utilizing amorphous wound cores," IEEE Transactions on Magnetics, vol. 46, no. 2, pp. 570–573 (2010)

(17) Z. Wang, R. Masaki, S. Morinaga, Y. Enomoto, H. Itabashi, M. Ito, and S. Tanigawa, "Development of an axial gap motor with amorphous metal cores," IEEE Transactions on Industry Applications, vol. 47, no. 3, pp. 1293–1299 (2011)

(18) R. A. Caamaˇno, "Electric motor or generator," U.S. Patent 5731649, Mar. 24 (1998)

(19) N. Ertugrul, R. Hasegawa, W. L. Soong, J. Gayler, S. Kloeden, and S. Kahourzade, "A novel tapered rotating electrical machine topology utilizing cut amorphous magnetic material," IEEE Transactions on Magnetics, vol. 51, no. 7, Art no. 8106006 (2015)

(20) T. Li, Y. Zhang, Y. Liang, Q. Ai, and H. Dou, "Multiphysics Analysis of an Axial-Flux In-Wheel Motor With an Amorphous Alloy Stator," IEEE Access, vol. 8, pp. 27414–27425 (2020)

(21) G. S. Liew, N. Ertugrul, W. L. Soong, J Gayler, "Investigation of axial field permanent magnet motor utilising amorphous magnetic material," Australian Journal of Electrical and Electronics Engineering, pp. 111-120 (2006)

(22) Hitachi News Release, "Highly Efficient Industrial 11kW Permanent Magnet

Synchronous Motor without Rare-earth Metals —Realizing IE4 Class Efficiency Standard with a Smaller Motor—," http://www.hitachi.com/New/cnews /120411.html (2014)

(23) Y. Enomoto, H. Tokoi, T. Imagawa, T. Suzuki, T. Obata, and K. Souma, "Amorphous motor with IE5 efficiency class," Hitachi Review, vol. 64, no. 8, pp. 480–487, (2015)

(24) T. Sano, M. Takahashi, Y. Murakoshi, and K. Matsuno, "Punchless blanking of an amorphous alloy," Journal of Materials Processing Technology, 30, 341-350, (1992)

(25) F. Luo, F. Sun, K. Li, F. Gong, X. Liang, X. Wu, and Jiang Ma, "Ultrasonic assisted micro-shear punching of amorphous alloy," Materials Research Letters, 6:10, pp. 545-551 (2018)

(26) H. Li, Y. Yan, F. Sun, K. Li, F. Luo, and Jiang Ma, " Shear Punching of Amorphous Alloys under High-Frequency Vibrations," 9(11), 1158 (2019)

(27) J. Cui, H. Liu, Y. Ma, M. Li, J. Gong, Y. Zhang, X. Wang, "Flexible microblanking of amorphous alloys under laser dynamic loading," Journal of Manufacturing Processes, 56, pp.718-725 (2020)

(28) F. Takahashi, T. Nishimura, I. Suzuki, and H. Kudo, "A Method of Blanking from Amorphous Alloy Foils Using Rubber Tool," Annals of the CIRP, Vol.40, no.1, pp.315-318 (1991)

(29) Y. Murakoshi, M. Takahashi, M. Terasaki, T. Sano, and K. Matsuno, "High-speed blanking of an amorphous alloy," Journal of Materials Processing Technology, 30, 329-339 (1992)

(30) J. Ou, Y. Liu, P. Breining, M. Schiefer, M. Doppelbauer, "Experimental Study of the Amorphous Magnetic Material for High-Speed Sleeve-Free PM Rotor Application," IEEE Transactions on Industrial Electronics, Vol.67, no.6, pp.4422-4432 (2020)

(31) T. Kumagai, H. Sakurai, J. Itoh, K. Kusaka, T. Yamaguchi, M. Nakagawa, D. Sato, "Experimental Evaluation of Characteristic of Switched Reluctance Motor Made by Blanking Amorphous Alloy Foil," The 23rd International Conference on Electrical Machines and Systems, LS2D-1, pp. 258-262 (2020)

(32) T. Matsuo, D. Shimode, Y. Terada, and M. Shimasaki, "Application of stop and play models to the representation of magnetic characteristics of silicon steel sheet," IEEE Transactions on Magnetics, Vol.39, no.3, pp.1361-1364 (2003)

(33) T. Matsuo and M. Shimasaki "An identification method of play model with input-dependent shape function," IEEE Transactions on Magnetics, Vol.41, no.10, pp.3112-43114 (2005)

(34) O. Bottauscio, M. Chiampi, and D. Chiarabaglio, "Advanced model of laminated magnetic cores for two-dimensional field analysis," IEEE Transactions on Magnetics, Vol.36, no.3, pp.561-573 (2000)

(35) K. Yamazaki and N. Fukushima, "Experimental validation of iron loss model for rotating machines based on direct eddy current analysis of electrical steel sheets," 2009 IEEE International Electric Machines and Drives Conference, pp.851-857 (2009)

(36) K. Narita, T. Asanuma, K. Semba, H. Sano, T. Yamada, K. Aiso, and K. Akatsu, "An accurate iron loss evaluation method based on finite element analysis for switched reluctance motors," 2015 IEEE Energy Conversion Congress and Exposition, pp. 4413-4417 (2020)

(37) T. Hara and K. Akatsu, "Comparison between analysis and experimental result of iron loss in SRM," The 23rd International Conference on Electrical Machines and Systems, LS3D-4, pp. 577-580 (2020)

(38) NIPPON STEEL CORPORATION: NON-ORIENTED ELECTRICAL STEEL SHEETS, https://www.nipponsteel.com/

(39) Hitachi Metals, Ltd.: AMORPHOUS ALLOY RIBBON Metglas, http://www.hitachi-metals.co.jp/

(40) N. Koga, S. Okada, and T. Yamaguchi, "Effect of Various Blanking Conditions on Properties of Cut Surface of Amorphous Alloy Foil and Tool Life," Journal of Japan Society for Technology of Plasticity, Vol.59, No.692, pp.176-180 (2018)

(41) Miller T. J. E.: Switched reluctance motors and their control, pp.161-180, Magna Physics Publications and Oxford University Press (1993)

(42) Y. Enomoto, K. Suzuki, S. Okita, K. Eto, and E. Katayama, "Evaluation of a Motor with an Amorphous Iron Core Punched by a Die," IEEJ Transaction on IA, Vol.141, No.5, pp.423-430 (2021)

Takahiro Kumagai (Student member) received the B.S. degree in electrical, electronics and information engineering from Nagaoka University of Technology, Niigata, Japan, in 2017, where he is currently working toward the Ph.D. degree. He is a student member of IEEJ and IEEE. His current research focuses on the driving method and the motor design method for switched reluctance motor.

Hirotaka Sakurai (Student member) received the B.S. degree in electrical, electronics and information engineering from Nagaoka University of Technology, Niigata, Japan, in 2021. He has been with Nagaoka University of Technology as a M.S. course student in electrical, electronics and information engineering. He is a student member of IEEJ and IEEE.

Taisuke Shioi (Student member) received the B.S. degree in electrical, electronics and information engineering from Nagaoka University of Technology, Niigata, Japan, in 2020. He has been with Nagaoka University of Technology as a M.S. course student in electrical, electronics and information engineering. He is a student member of IEEJ and IEEE.

Hirotaka kato (Student member) is currently working for the B.S. degree in electrical, electronics and information engineering from Nagaoka University of Technology, Niigata, Japan. He is a student member of IEEJ.

Jun-ichi Itoh (Senior member) received his M.S. and Ph.D. degree in electrical and electronic systems engineering from Nagaoka University of Technology, Niigata, Japan in 1996, 2000, respectively. From 1996 to 2004, he was with Fuji Electric Corporate Research and Development Ltd., Tokyo, Japan. He was with Nagaoka University of Technology, Niigata, Japan as an associate professor. Since 2017, he has been a professor. His research interests are matrix converters, dc/dc converters, power factor correction techniques, energy storage system and adjustable speed drive systems. He received IEEJ Academic Promotion Award (IEEJ Technical Development Award) in 2007. In addition, he also received Isao Takahashi Power Electronics Award in IPEC-Sapporo 2010 from IEEJ, 58th OHM Technology Award from The Foundation for Electrical Science and Engineering, November, 2011, Intelligent Cosmos Award from Intelligent Cosmos Foundation for the Promotion of Science, May, 2012, and Third prize award from Energy Conversion Congress and Exposition-Asia, June, 2013. Prizes for Science and Technology (Development Category) from the Commendation for Science and Technology by the Minister of Education, Culture, Sports, Science and Technology, April 2017. He is a senior member of the Institute of Electrical Engineers of Japan, the Society of Automotive Engineers of Japan and the Institute of Electrical and Electronics Engineers.

Keisuke Kusaka (Member) received the B.S. and M.S. degrees in electrical, electronics and information from Nagaoka University of Technology, Niigata, Japan in 2011, 2013, respectively. From 2015 to 2016, he was with Swiss Federal Institute of Technology in Lausanne (EPFL), Switzerland as a trainee. In 2016, he received the Ph.D. degree in energy and environment science from Nagaoka University of Technology. He was with Nagaoka University of Technology, Niigata, Japan as a researcher from 2016 to 2018. Since 2018, he has been with Nagaoka University of Technology, Niigata, Japan as an assistant professor. His current research interests include the areas of IPT systems and high-frequency converters. He is a member of Institute of Electrical Engineers of Japan, Society of Automotive Engineers of Japan and the IEEE.

Takashi Yamaguchi (Non-Member) is currently Chief Executive Officer with Yamaguchi Manufacturing Co., Ltd. He is engage in precision mold manufacturing and precision press processing.

Masayuki Nakagawa (Non-Member) joined Industrial Research Institute of Niigata Prefecture in 1996. He currently belongs to the Research and Development Center. He is engaged in measurement and analysis work requested by companies, including research on metal joining and surface modification.

Daisuke Sato (Member) received the B.S. and M.S. degrees in electrical, electronics and information from Nagaoka University of Technology, Niigata, Japan in 2012, 2014, respectively. In August 2016, he established Nagaoka Motor Development Co., Ltd. In 2017, he received the Ph.D. degree in energy and environment science from Nagaoka University of Technology. His current research interests include the areas of rotating machines.